Soft Matter



PAPER View Article Online
View Journal | View Issue



Cite this: *Soft Matter*, 2022, **18**, 6254

Received 2nd May 2022, Accepted 2nd August 2022

DOI: 10.1039/d2sm00564f

rsc.li/soft-matter-journal

Hysteresis in the thermally induced phase transition of cellulose ethers†

Navid Bizmark, (10 *ab Nicholas J. Caggiano, (10 ‡b Jason X. Liu, (10 ‡ac Craig B. Arnold, bc Robert K. Prud'homme, (10 b Sujit S. Datta (10 b and Rodney D. Priestley (10 *ab)

Functionalized cellulosics have shown promise as naturally derived thermoresponsive gelling agents. However, the dynamics of thermally induced phase transitions of these polymers at the lower critical solution temperature (LCST) are not fully understood. Here, with experiments and theoretical considerations, we address how molecular architecture dictates the mechanisms and dynamics of phase transitions for cellulose ethers. Above the LCST, we show that hydroxypropyl substituents favor the spontaneous formation of liquid droplets, whereas methyl substituents induce fibril formation through diffusive growth. In celluloses which contain both methyl and hydroxypropyl substituents, fibrillation initiates after liquid droplet formation, suppressing the fibril growth to a sub-diffusive rate. Unlike for liquid droplets, the dissolution of fibrils back into the solvated state occurs with significant thermal hysteresis. We tune this hysteresis by altering the content of substituted hydroxypropyl moieties. This work provides a systematic study to decouple competing mechanisms during the phase transition of multi-functionalized macromolecules.

Introduction

Cellulose ethers have been used as promising gelling agents in diverse biomedical, environmental, and pharmaceutical settings. Their natural origin, together with their responsive behavior to external triggers, has made them viable candidates in the production of smart materials $^{6\text{--}10}$ which reduce our reliance on hydrocarbon resources and our carbon footprint. The stimuli-responsive behavior of cellulosic derivatives originates from their molecular architecture. Native cellulose is composed of glucose monomers joined by $\beta\text{--}1,4$ linkages the interand intramolecular hydrogen bonds between the three hydroxyl groups per glucose monomer. These strong molecular bonds form crystalline structures which render cellulose

insoluble in most common solvents. ^{13–17} Chemical functionalization of cellulose, namely alkylation, disrupts the crystallinity of native cellulose by substituting the hydroxyl groups with alkyl and/or hydroxyalkyl groups, yielding cellulose ethers such as methyl cellulose (MC), hydroxypropyl cellulose (HPC), and hydroxypropyl methylcellulose (HPMC) (see Fig. 1). ¹⁸ The number of substituted hydroxyl groups per monomer in modified celluloses is defined as the degree of substitution (DS), which can vary between 0 (no substitution) and 3 (maximum substitution). The substituent chemistry and DS are key factors

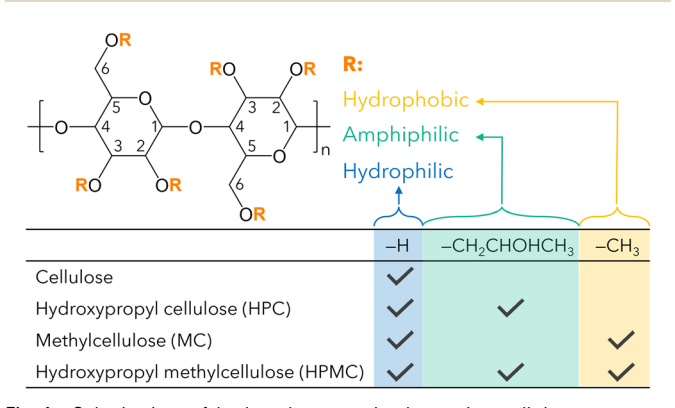


Fig. 1 Substitution of hydroxyl groups in the native cellulose structure with methyl and hydroxypropyl groups through alkylation to produce methyl cellulose, hydroxypropyl cellulose, and hydroxypropyl methylcellulose.

^a Princeton Institute for the Science and Technology of Materials, Princeton University, Princeton, New Jersey 08544, USA. E-mail: nbizmark@princeton.edu, rpriestl@princeton.edu

^b Department of Chemical and Biological Engineering, Princeton University, Princeton, New Jersey 08544, USA

^c Department of Mechanical and Aerospace Engineering, Princeton University, Princeton. New Iersev 08544. USA

 $[\]dagger$ Electronic supplementary information (ESI) available: Estimates of free energy of mixing for different $\chi_{\rm p-s}$, estimates of volume fraction of polymer in the condensate phase, angular dependency of scattered light for HPC globules and MC fibrils, estimates of overlap concentration, C^* , for HPC and MC, DLS correlation functions and the fits (file type, PDF). See DOI: https://doi.org/10.1039/d2sm00564f

[‡] Contributed equally.

which dictate the rheological, interfacial, and thermal properties of cellulose ethers. 18,19 These factors also influence solubility; for example, MC is soluble in water when the DS is greater than 1.5,20 whereas ethyl cellulose is water-soluble only when the DS is less than 1.5. 18,21

At or above the lower critical solution temperature (LCST), HPC, MC, and HPMC exhibit thermoresponsive behavior due to the presence of amphiphilic and hydrophobic substituents. At or above the LCST, these polymers transition from a soluble to an insoluble state in water, followed by gelation if at sufficiently high polymer concentrations. 22-25 While for other macromolecules, such as block copolymers, the hydrophilic-tohydrophobic and gelation transitions have been characterized extensively via the careful tuning of polymer architecture, 26-34 the phase transition of cellulose ethers remains largely unexplored. This is largely due to the non-selective nature of the alkylation, which results in a wide variety of molecular architectures. For example, MC with an average DS of 2 comprises approximately 30%, 39%, and 26% glucose monomers with tri-, di-, and mono-substituted methyl groups, respectively, with \sim 5% glucose monomers in their native form. ^{22,35}

Substituent chemistry significantly impacts the phase transition mechanisms of cellulose ethers, dictating their gelling behavior at elevated temperatures. For HPC, spinodal decomposition has been proposed as the mechanism of gelation, ^{36,37} while cryogenic transmission electron microscopy (cryo-TEM) imaging has revealed that MC gels are composed of fibrillar networks. 23,38-40 MC fibrillation is believed to follow a multiscale hierarchical self-assembly pathway initiated from nucleation.²² MC fibrils, with possibly crystalline internal structures, 41 are found to have a diameter of 15-50 nm^{23,38,40} independent of MC molecular weight and concentration. 42 In the absence of experimental evidence, molecular dynamics simulations 43-47 have suggested the assembly of MC into different nuclei conformations from which fibrils can grow. This growth is driven by rapid (O(10⁻⁹ s)) conformational change of phase separated chains to obtain fibrillar structures. However, there is still debate surrounding the mechanisms and kinetics of phase separation and fibrillation of cellulose ethers.22

The two different phase transition mechanisms of HPC and MC suggest that HPMC, which contains both methyl and hydroxypropyl substituents, may exhibit complex thermoresponsive behavior. Like HPC,³⁷ a sharp reduction in the storage and loss moduli of aqueous solutions of HPMC has been observed prior to gelation. 23,48,49 However, cryo-TEM images of HPMC solutions above the LCST have demonstrated the formation of HPMC fibrils similar to those formed by MC. 48 This unique gelling behavior of HPMC is thought to originate from complex interactions between the polymer backbone, side chains, and water molecules. To investigate such interactions, experimental50 and computational51 studies have shown that the presence of grafted hydrophilic poly(ethylene glycol) chains on the MC backbone can suppress fibrillation and gelation at elevated temperatures.

Here, we experimentally demonstrate the impact of substituent chemistry on the thermoresponsive behavior of cellulose

ethers in aqueous solution. Specifically, we aim to understand the competition between two possible mechanisms during the phase transition of HPMC: (i) liquid-liquid phase separation and (ii) nucleation and fibrillation. In order to decouple the dynamics of the phase transition from those of gelation, we conduct all experiments on very dilute solutions (0.01 to 0.1 wt%) unless otherwise noted. Through liquid-phase differential scanning calorimetry (DSC) and long-duration dynamic light scattering (DLS) measurements, we demonstrate—in line with a recently proposed mechanism⁴⁸—that the phase separation of HPMC initiates with liquid droplet formation, which is followed by fibrillation from the liquid droplets. By varying the hydrophilic-to-hydrophobic substituent ratios, we systematically explore the thermoresponsive behavior of HPMC during heating and cooling. We show that increasing the content of amphiphilic moieties (i.e., hydroxypropyl) in HPMC reduces the thermal hysteresis observed between heating and cooling periods. At two extreme conditions, hysteresis is absent for HPC (with only amphiphilic substituents) while it is the greatest for MC (with only hydrophobic substituents). This approach will enable a systematic deconvolution of competing mechanisms during the phase transition of multi-functionalized macromolecules.

Results and discussion

Controlling and conceptualizing the hysteresis between heating and cooling

Cellulose ethers used in this study (HPC, MC, and HPMC) were provided in a wide range of molecular weights (MWs) by Shin Etsu Chemical Co. (see Table 1 in Materials and methods). DLS measurements in which we thermally cycled the aqueous solutions between 30 and 80 °C were conducted on very dilute (0.025 wt%) agueous solutions of these macromolecules to explore the effects of substituent chemistry on thermoresponsive dynamics. Fig. 2A shows the characteristic length of HPC, MC, and HPMC precipitates (see Materials and methods),

Table 1 Properties of different grades of HPC, MC, and HPMC used in this work. Unspecified molecular weight (MW), viscosities (2% aqueous solutions at 20 °C), methoxy, and hydroxypropoxy contents, degree of substitution (DS), and molar substitution (MS) for HPC 53 and MC/HPMC 63 were provided by the manufacturers. The polydispersity index for MW of HPC and MC was $<3^{64}$ and <5, 63 respectively

	Trade name	Viscosity (mPa s)		Methoxy content (wt%)	Hydroxypropoxy content (wt%)
HPC	HPC-SSL	2.5	40	N/A	73.0 (MS = 3.6)
	HPC-L	7.6	140		74.6 (MS = 3.8)
	HPC-M	306	700		74.5 (MS = 3.8)
	HPC-H	2210	1000		75.8 (MS = 3.9)
	HPC-VH	5040	2500		75.1 (MS = 3.8)
MC	SM-25	22.7	85	29.2 (DS = 1.9)	N/A
	SM-100	104	150	29.3 (DS = 1.9)	
	SM-400	473	200	29.2 (DS = 1.9)	
	SM-4000	4980	400	29.4 (DS = 1.9)	
	SM-8000	7700	500	30.3 (DS = 2.0)	
HPMC	65SH-	4740	350	27.9 (DS = 1.8)	6.2 (MS = 0.15)
	4000			` ,	, ,
	60SH-	4570	350	28.7 (DS = 1.9)	8.8 (MS = 0.25)
	4000			, ,	` ,

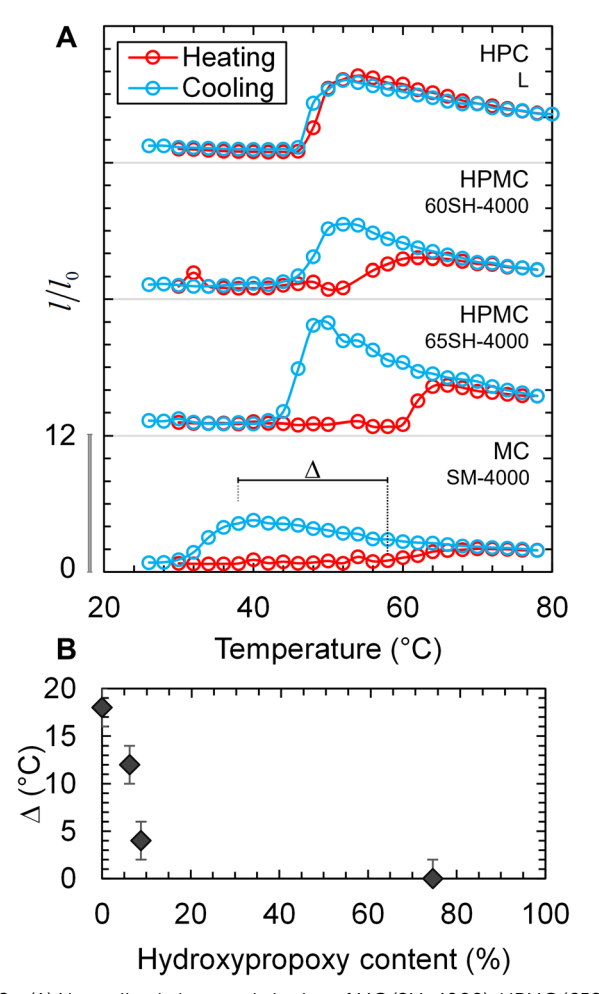


Fig. 2 (A) Normalized characteristic size of MC (SM-4000), HPMC (65SH-4000 and 60SH-4000), and HPC-L all with close MW (see Table 1). The heating and cooling rates were 0.2 °C min⁻¹ and the aqueous polymer concentration was 0.025 wt%. Characteristic lengths (I) have been normalized by the initial length (l_0) at their corresponding LCST. (B) The difference in onset temperatures (Δ) at which the phase transition during heating and cooling happened as a function of hydroxypropyl content in MC, HPMC, and HPC in (A). The reported errors in (B) are ± 2 °C, which were obtained from the temperature step change during heating and cooling.

l, relative to that at the LCST, l_0 , where $\frac{l}{l_0}$ is a comparative measure of the state of the polymer: solvated, condensed, or hydrated. The LCST for each polymer solution has been determined from turbidity measurements, discussed in the following sections. We find that the phase transition of HPC during heating and cooling occurred with no hysteresis, whereas a significantly large thermal hysteresis ($\Delta = 18$ °C) was observed for MC as shown in Fig. 2B. This difference suggests that the presence of amphiphilic segments (i.e., hydroxypropyl) may control the dynamics of the thermally induced phase transition of cellulose ethers. We further examined this idea by tracking the size changes of HPMC during heating and cooling. In line with our hypothesis, Fig. 2A and B reveal that the hysteresis in HPMC was reduced as hydroxypropyl content was increased.

Fig. 2A shows that the transition from above the LCST is sharp for HPC, whereas it is gradual for MC. Transmittance measurements in Fig. 3A and B address these two transition dynamics for dilute concentrations of HPC and MC, respectively, over a range of temperatures. As temperature increased from 30 °C to 80 °C at a rate of 0.2 °C min⁻¹, the HPC and MC solutions underwent a transition from transparent to opaque, corresponding to an LCST of 46 \pm 2 $^{\circ}$ C and 59 \pm 2 $^{\circ}$ C, respectively. Like the size measurements in Fig. 2A, the reduction of transmittance above the LCST is sharp for HPC, whereas it is gradual for MC. Due to the slow nature of the MC phase transition near the LCST, a substantially long time might be required to be able to detect the phase separation. For example, light scattering measurements have revealed the phase separation of MC aged at 40 °C for 12 days.³⁹

The large distinction in the phase transition dynamics and the LCST values for HPC and MC suggests a mechanistic difference in the phase separation of these two polymers. In agreement with these expectations, atomic force microscopy (AFM) reveals two drastically different morphologies of the phase separated HPC and MC. While MC formed fibrils, as observed before, 23,38,40,52 HPC polymers phase separated into liquid droplets (see Fig. 3C). In the following sections, we elaborate plausible mechanisms to explain the two different phase transition behaviors and dynamics for HPC and MC, leading to understand the phase transition behavior of HPMC.

HPC droplet formation

Phase-separated HPC droplets are formed at temperatures above the LCST. From transmittance measurements shown in Fig. 3A, we find that the LCST is 44-46 °C for HPC with a MW of $\sim 1000 \text{ kg mol}^{-1}$ (labeled as HPC-H, see Materials and methods). Independently, DLS measurements in Fig. 4A similarly reveal that the phase transition begins at temperatures just above 44 °C, seen as an abrupt jump in the size measurements. Between 44-48 °C, the phase-separated liquid drops remain near their maximum size, followed by a gradual size decrease as the temperature increases above 48 °C. This dynamic behavior suggests that the HPC liquid droplets remain fully hydrated within the range of 44-48 °C but begin to dehydrate above 48 °C. Such water expulsion from HPC droplets results in significant shrinkage (~90%) in droplet volume compared to their hydrated state at 44-48 °C. This strong sensitivity to hydration is completely reversible. When the temperature is decreased from 80 °C to 46 °C, HPC droplets gradually re-hydrate to the initial sizes that were obtained during heating. Then, within just 2 °C from the peak of the transition at 46 °C, the droplets completely dissolve into free polymer chains. Thus, there is a negligible thermal hysteresis in the phase transition of HPC during heating and cooling.

We further elucidated the mechanism and reversibility of the phase separation of HPC by conducting liquid-phase DSC using high volume hermetically sealed pans. Fig. 4B shows the heat flow to an aqueous solution of HPC-H (2.6 wt%). The heating rate was 1 °C min⁻¹ to ensure quasi-steady-state measurements. Interestingly, the heating thermogram for

Paper

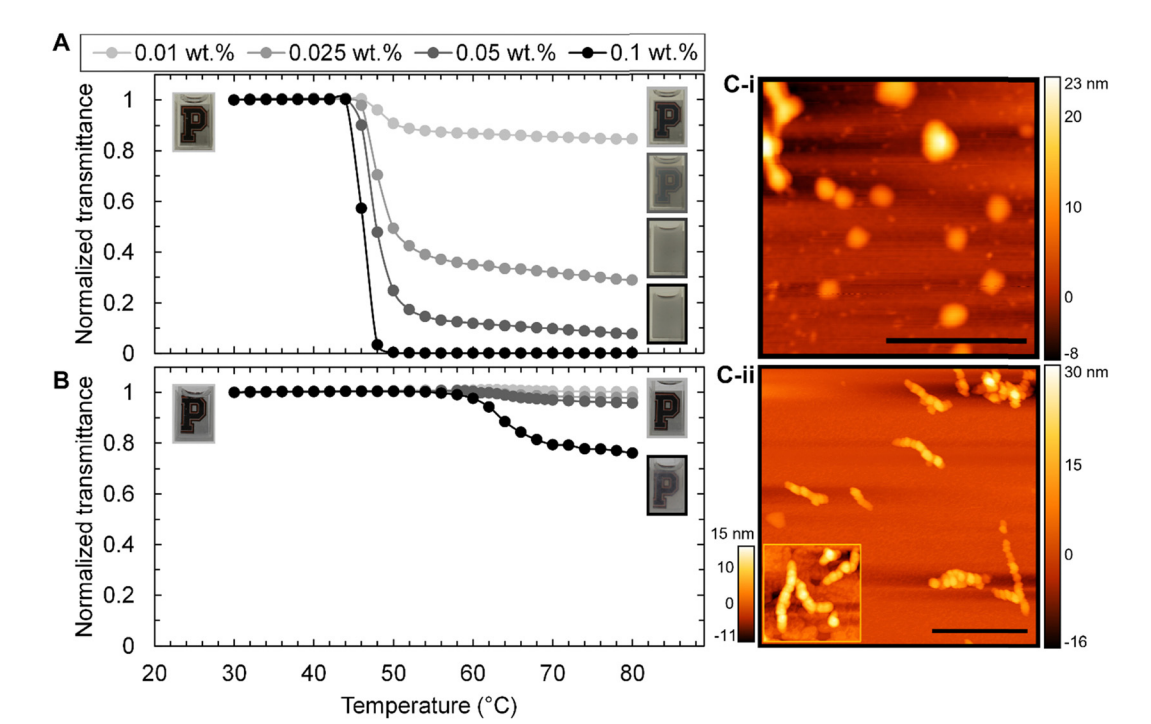


Fig. 3 (A and B) Transmittance measurements for aqueous solutions of HPC (1000 kg mol⁻¹) and MC (500 kg mol⁻¹), respectively, at a concentration range between 0.01 wt% and 0.1 wt%. At each concentration, the transmittance is normalized by the initial transmittance measured at 30 °C. The aqueous solutions were heated at a constant rate of 0.2 °C min⁻¹. The corresponding visual liquid transparency is shown for each case. (C) AFM images of HPC droplets (i) and MC fibrils (ii) deposited on silicon wafers at 70 $^{\circ}$ C. Scale bar in (C) is 1 μ m.

HPC-H revealed two main steps during the thermally induced phase transition: an intermediate phase transition initiated at 44 °C followed by a sharp endothermic transition at ~ 50 °C. Based on the prior DLS measurements, the hydrated state of the HPC droplets is reflected by the intermediate step between 44-48 °C, which appears as a shoulder in the thermogram (see Fig. 4B). Remarkably, as the temperature increases beyond 48 °C, the expulsion of water from the droplets results in a sizeable endothermic peak at \sim 50 °C. This may be attributed to the weakening of hydrogen bonds between the hydroxyl groups in the side chains of HPC and water molecules.

Fig. 4A and B show that during cooling from 80 °C to 45 °C, HPC droplets continuously swell until they exothermally dissolve into free polymer chains at temperatures below 45 °C, thus releasing the same energy that was consumed during heating (equal areas under the heating and cooling curves). To understand the reversibility of the process more rigorously, we conducted the DSC heating-cooling cycles for specific temperature ranges: (i) 20-50 °C and (ii) 20-53 °C, shown in Fig. 4C-i and ii, respectively. From DLS measurements, when the heating takes place up to 47 $^{\circ}$ C, HPC-H polymer chains are expected to phase separate into hydrated liquid droplets. When the heating continues to the water expulsion point at 50 °C and beyond, as shown in Fig. 4C, an exothermic transition with a peak at 45 °C is observed during cooling.

Our interpretations of the DSC thermograms corroborate the interplay between the phase separation and gelation. Instead of phase separation and gelation occurring simultaneously, HPC

first phase separates, then transitions to a gel as the temperature continues to increase. This results in a thermal gap in the gelation process. 37,49 To explore this idea, we assessed the phase transition of commercially available HPC grades of different MW by DSC and DLS. Fig. 5A shows the heat flow to aqueous solutions of HPC (2.6 wt%) with MW of 40 kg mol^{-1} 140 kg mol^{-1} , 700 kg mol^{-1} , 1000 kg mol^{-1} , and 2500 kg mol^{-1} . This concentration is above the overlap concentration of each HPC grade, satisfying the gelation condition during the phase transition (see Table S1 in the ESI†). As in Fig. 4B, the heating rate was 1 °C min⁻¹ to ensure quasi-steady-state measurements. We observe that as MW decreases, the shoulder region in the thermograms also decreases in width; the highest MW (2500 kg mol⁻¹) displays the widest shoulder, while the two lowest MWs (40 kg mol⁻¹ and 140 kg mol⁻¹) display no shoulder. This trend can be attributed to the polymer's affinity to water. At low MWs, the proposed successive transitiongelation mechanism does not occur for 2.6 wt% solutions since the phase-separated HPC droplets remain hydrated due to their high affinity to water. For high MW HPC, a thermal gap between phase separation and gelation is evident, thus suggesting a dual phase transition gelation mechanism.49

In a qualitative agreement with theoretical considerations using Flory Huggins solution theory (see the ESI†), HPC polymer chains of all grades condense first into polymer-rich droplets at the LCST (the onset temperature in Fig. 5A) corresponding to a critical χ_{p-s} (χ_{p-s}^*), where χ_{p-s} is the effective 20

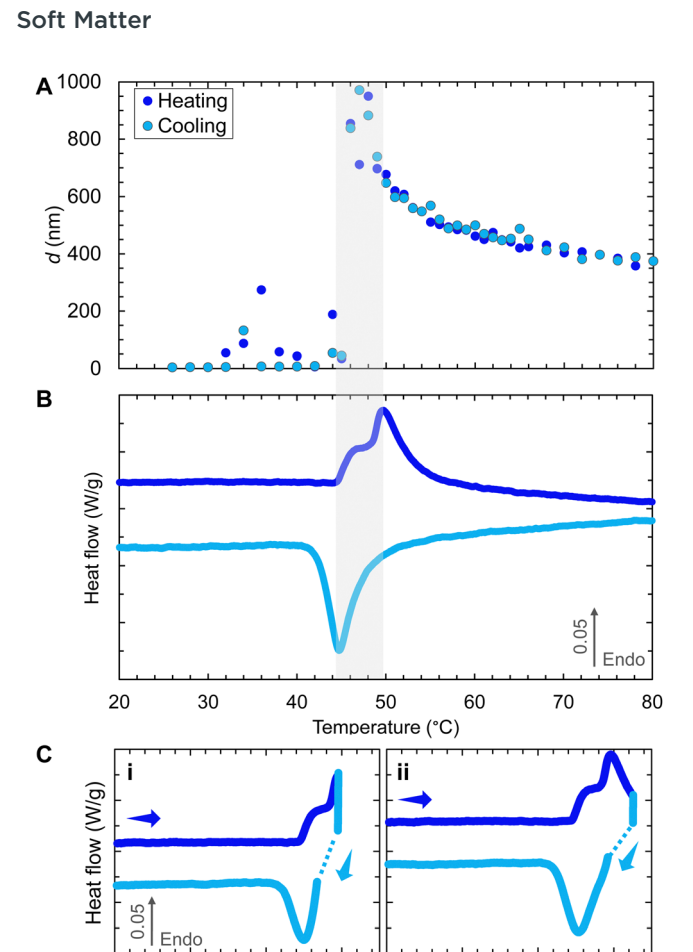


Fig. 4 (A) Changes in the diameter, d, of HPC (1000 kg mol $^{-1}$) dissolved in water at a concentration of 0.025 wt% during heating from 30 to 80 °C and cooling from 80 to 26 °C, both at a rate of 0.2 °C min $^{-1}$. (B) DSC measurements of an aqueous solution of 2.6 wt% HPC during heating and cooling between 20–80 °C at a rate of 1 °C min $^{-1}$. The shaded area in (A) and (B) represents the temperature range during the phase transition. (C) DSC measurements similar to that in (B) but within a temperature range of (i) 20–50 °C and (ii) 20–53 °C. The upward arrow in (B) and (C) shows the endothermic direction with the corresponding magnitude of heat flow. For a clearer visualization, the cooling curves in (B) and (C) are vertically shifted up and the truncated data points are shown in dotted lines.

50 20

40

Temperature (°C)

50

40

Temperature (°C)

polymer–solvent interaction parameter. Due to the higher solubility of low MW HPC in water, ⁵³ we expected that the phase transition for low MW HPC would occur at a higher temperature than for high MW HPC. This dynamic behavior is directly reflected in the binary phase diagram for a given MW and χ_{p-s} . When $\chi_{p-s} > \chi_{p-s}^*$, condensate (α) and water (β) phases are formed in which the volume fraction of polymer is ϕ_p^{α} and ϕ_p^{β} , respectively. These two points are at equilibrium on the binary phase curve with a common tangent (see Fig. S1A, ESI†). As χ_{p-s} increases, they move apart from each other (see Fig. S1 in the ESI†). This increase in χ_{p-s} drives the energetically favorable transition from initial polymer-rich droplets to final dehydrated spheres. Nevertheless, for a given large χ_{p-s} (e.g., 1.6) droplets of high MW are more dehydrated than those of low MW (see Fig. S1B in the ESI†). This theoretical expectation

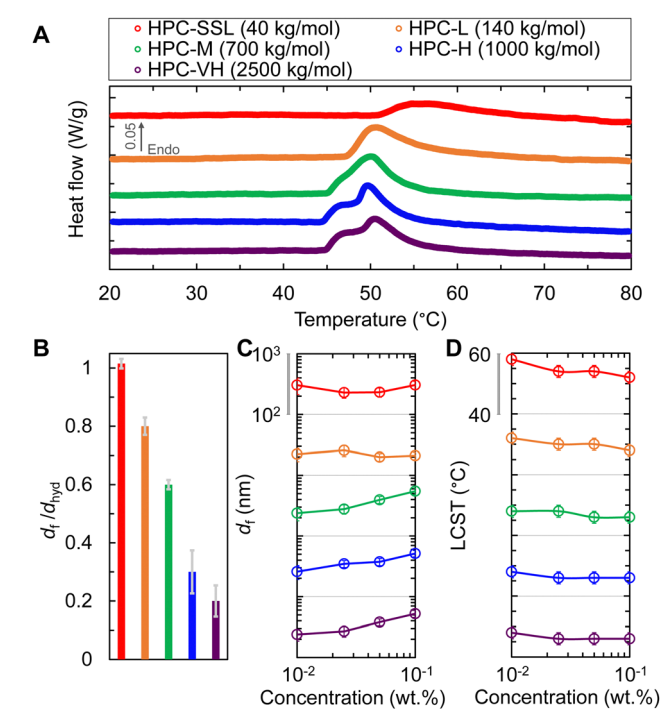


Fig. 5 (A) DSC measurements of aqueous solutions of 2.6 wt% HPC at various molecular weights: 40 kg mol^{-1} (HPC-SSL), 140 kg mol^{-1} (HPC-L), 700 kg mol^{-1} (HPC-M), 1000 kg mol^{-1} (HPC-H), and 2500 kg mol^{-1} (HPC-VH). The heating and cooling rate was $1 \,^{\circ}\text{C}$ min $^{-1}$, and the upward arrow shows the endothermic direction and the magnitude of heat flow. (B) Hydrodynamic diameter of HPC droplets at $80 \,^{\circ}\text{C}$ (d_{t}) normalized by the corresponding diameter at the hydrated state (d_{hyd}). The HPC droplets at both stages (d_{hyd} and d_{t}) were monodispersed (PDI < 0.25) at all MWs. Polymer concentration in (B) has been 0.025 wt%. (C) d_{f} and (D) LCST for different grades of HPC shown in (A) at different concentrations within 0.01 to 0.1 wt%.

is quantitatively supported by experimental results shown in Fig. 5B for dilute aqueous solutions of HPC. Here, the polymerrich liquid droplets of low MW (40 and 140 kg mol⁻¹) at 80 °C shrink marginally from their hydrated state at the LCST, whereas the shrinkage is more significant by at least a factor of two in diameter for high MW (1000 and 2500 kg mol⁻¹) HPC-H and VH droplets.

We systematically varied the concentration of HPC to elucidate its possible influence on droplet formation during precipitation.⁵⁴ Fig. 5C and D show the diameter of HPC droplets (d_f) obtained at 80 °C and at the LCST, respectively, for all MWs shown in Fig. 5A, at polymer concentrations from 0.01 to 0.1 wt%. Unlike the LCST, which decreases as concentration increases for all MWs, we find that df remains essentially unchanged for low MW HPC grades but increases with polymer concentration when MW is large. We expected the size of droplets to be influenced by the polymer concentration above the overlap concentration, C^* (see Table S1 in the ESI \dagger), where gelation is possible. This occurs for HPC-M, -H, and -VH where the polymer concentrations exceeded the corresponding C*. However, the tested concentrations for HPC-SSL and -L were less than C^* , and as a result, the HPC droplet diameter did not depend on polymer concentration.

MC fibril formation

Paper

Unlike HPC, MC polymer chains nucleate and form fibrillar structures during the thermally induced phase transition (see Fig. 3C-ii). This transition is gradual, as reflected by the broad range of temperatures over which the transmittance decreases as well as by the appearance of a broad endothermic peak in the DSC thermogram, shown in Fig. 3B and 6A, respectively. The gradual changes that occur during these phase transitions suggest that MC fibrillation is kinetically controlled. Previous studies have demonstrated that the length of MC fibrils is strongly correlated with MW42 while their width remains relatively constant, between 15-50 nm in diameter, 23,38,40 independent of the MW and concentration. 42 Fig. 6B shows the characteristic length of MC fibrils (see Materials and methods), l, at a given temperature normalized by that at the LCST, l_0 . This normalization was required since the absolute length of asymmetric objects, including MC fibrils, cannot be directly measured by dynamic light scattering techniques; only their relative lengths can be obtained (see Materials and methods). For MC with a MW of 400 kg mol⁻¹ at a concentration of 0.025 wt% (below C^* , see Table S1 in the ESI†), we find that the MC fibrils begin to form above 56 °C and continue to grow as heating continues to 70 °C at a rate of 0.2 °C min⁻¹. Beyond 70 °C, the length of MC fibrils remained unchanged, ruling out the possibility of gelation at this low polymer concentration. In line with earlier calorimetry studies,⁵⁵ the DSC thermograms for both HPC (Fig. 4B) and MC (Fig. 6A) suggest that hydrogen bonds between the cellulose ethers and water molecules break up during heating. In this process, water molecules undergo a conformational change from an ordered state to a random state, resulting in a positive entropy change, and thus, an endothermic peak. During cooling, the process occurs in reverse, undergoing an exothermic transition. Unlike HPC droplets, a

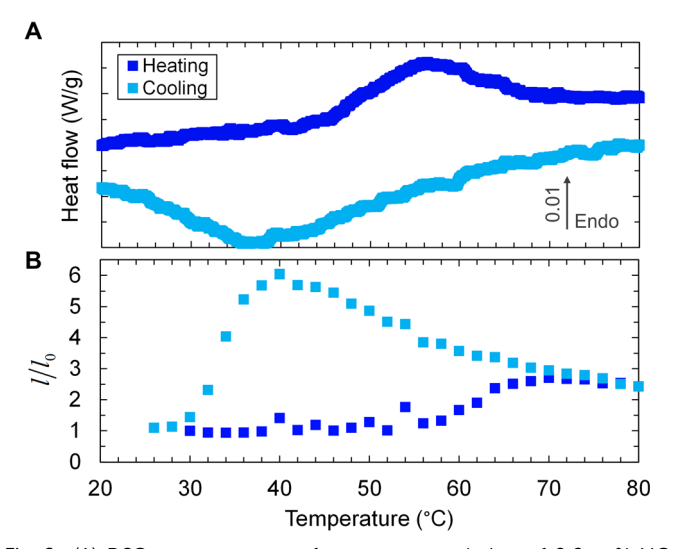


Fig. 6 (A) DSC measurements of an aqueous solution of 2.6 wt% MC (400 kg mol⁻¹) during heating and cooling between 20-80 °C at a rate of 1 °C min⁻¹. (B) Changes in the representative length (I) of MC within 20-80 °C normalized by the length (l_0) at LCST (i.e., 56 °C). MC concentration was 0.025 wt% and the heating/cooling rates were both at 0.2 °C min⁻¹.

significant hysteresis was observed in the calorimetry and size measurements of MC fibrils during the cooling period (see Fig. 6A and B) as well as in previous rheological studies. 22-25,38,39,52 Such hysteresis has also been reported for protein systems⁵⁶ as well as the dissolution of drugs in a liquid medium.⁵⁷ It is proposed that the dissolution mechanism of polymers involves solvent diffusion and polymer chain disentanglement.⁵⁸ In line with this proposed mechanism, we show in Fig. 4A and 6B that the size of HPC droplets and MC fibrils, respectively, increases during the cooling from 80 °C to a critical point below which polymers completely dissociated into free chains.

Molecular simulations^{44,47} have suggested that MC nuclei undergo rapid conformational fluctuations within which drive fibrillar growth at sufficiently large concentrations. Following a plausible multiscale fibrillation growth mechanism, we assume that the phase transition of very dilute solutions of MC initiates with nucleation, after which chains diffuse slowly to find each other and form fibrils. Therefore, in such dilute systems the overall fibril growth is controlled via a slow diffusive process. We tracked the change of $\frac{l}{l_0}$ for different MW of MC during heating and cooling periods at a constant rate of 0.2 °C min⁻¹, shown in Fig. 7A. As expected, we find that the LCST (the onset temperature during the heating cycles at which $\frac{l}{l_0}$ begins to monotonically increase) decreases with increasing MW (see Fig. 7B). Moreover, like HPC liquid droplets, the rehydration of MC fibrils during cooling is more pronounced when MW is smaller.

Fibril growth via a diffusive condensation process is expected when the energy barrier for nucleation is overcome at or above the LCST. Therefore, when maintaining the temperature of polymer solution at the LCST, we expect that fibrils continuously grow through the diffusive condensation of polymer chains from bulk into a fibrillar structure. Since the fibril growth is very slow, extensive isothermal aging to reach the hydrated state is not feasible. Instead, we obtained the hydrated state of fibrils during the cooling period (see the upward arrow in Fig. 7A). We define $\bar{l} \equiv \frac{l}{l_{\rm max}}$, where l is the characteristic length of MC fibrils at the LCST, which increases isothermally in time from l_0 to a maximum size of l_{max} at the hydrated state. We propose the long-term MC fibrillation growth rate at a constant temperature to be in the general form of $\frac{dl}{dt} = kt^{\alpha}$. Here, k and α are rate constants that may vary with polymer concentration, MW, and temperature. By integrating the proposed rate and applying the initial condition of $\bar{l} = \frac{l_0}{l_{\text{max}}}$ at

t = 0, we obtain $\frac{l(t) - l_0}{l_{\text{max}}} = At^B$, where A and B are constant.

To examine the prediction of our proposed kinetic model, 0.025 wt% aqueous solutions of MC were heated to their respective LCSTs (obtained from the measurements in Fig. 7A).

Subsequently, we measured $\frac{l(t)}{l_0}$ over several hours while

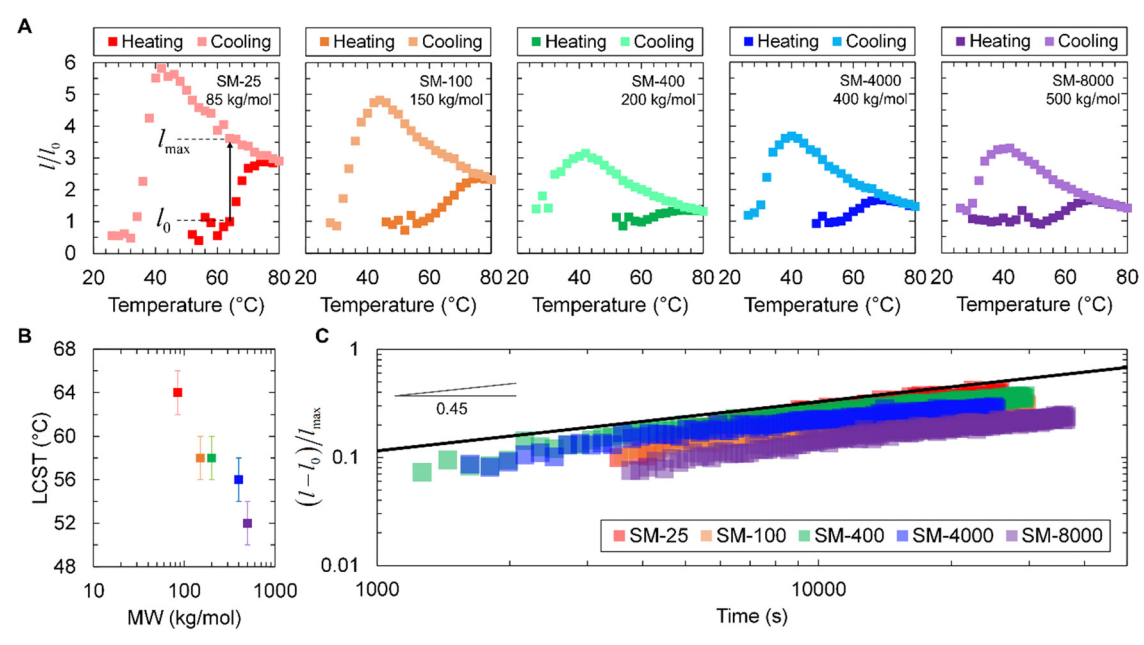


Fig. 7 (A) Changes in the characteristic length (I) of MC as a function of temperature for five different MWs normalized by the initial length (I_n) at their corresponding LCST. The concentration of polymers was 0.025 wt% in all cases, and the heating/cooling rates were both at 0.2 °C min⁻¹. (B) The LCST as a function of MW for MC grades shown in (A). The reported errors are ± 2 °C, which were obtained from temperature step change during heating and cooling. (C) The isothermal growth rate of MC fibrils shown in (A) from l_0 to l_{max} at their corresponding LCST, see the upward arrow in (A). The solid line in (C) shows $(l - l_0)/l_{\text{max}} \sim t^{0.45}$

maintaining the temperature constant at the LCST. Under these conditions, the energy barrier of nucleation is expected to be overcome, making diffusion the predominant mechanism of fibril growth. Fig. 7C shows how $\frac{l(t)-l_0}{l_{\max}}$ varies with time for all grades of MC. We find that for all tested MW, the power B remains within a range of 0.45 \pm 0.06, suggesting that the growth rate is controlled by the diffusion of nucleated polymers from bulk solution into the condensed phase.

We employ our understanding of the phase transition

Phase transition mechanism of HPMC

dynamics of HPC and MC to explain the thermoresponsive behavior of HPMC. Like HPC, the presence of hydroxypropyl substituent in HPMC drives liquid-liquid phase separation at the LCST. This expectation is reflected by the substantial jump in measured size during the heating periods (shown in Fig. 2A). However, unlike HPC, fibrillar structures may grow from the HPMC liquid droplets due to the interplay of interactions of methyl side chains with other side chains and the backbone.⁵¹ Growth of fibrils from liquid HPMC droplets is expected to be limited, yielding smaller fibrils than those from MC. 48 We observe that during the isothermal fibrillation of HPMC, $\frac{l(t)-l_0}{l_{\max}}$ reaches a plateau at longer times, supporting our expectation of limited fibrillation from the liquid droplet. Moreover, the smaller power B for HPMC compared to that for MC (see Fig. 8) suggests slower fibrillation kinetics due to different fibrillation pathways: HPMC fibrillation from liquid droplets vs. MC fibrillation from bulk solution. The formation of physical entanglements between

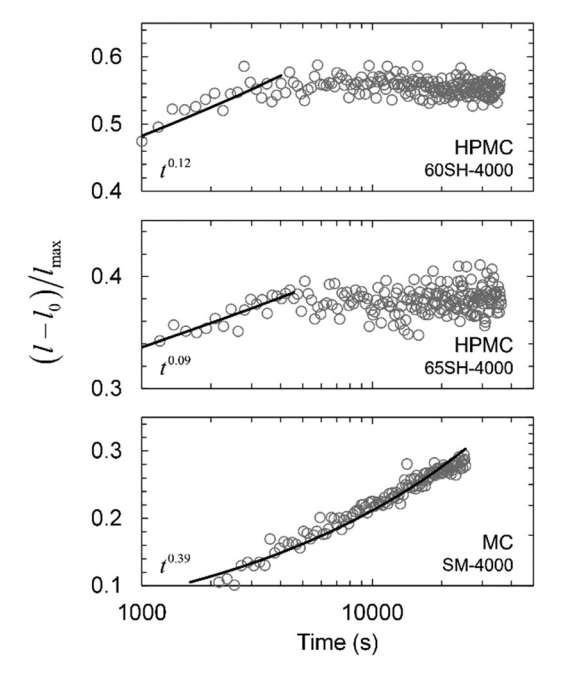


Fig. 8 The isothermal growth rate of MC and HPMC fibrils shown in Fig. 2 from l_0 to l_{max} at their corresponding LCST, as shown with the upward arrow in Fig. 7A. The solid lines are the power-law fits $(l - l_0)/l_{\text{max}} \sim t^B$.

polymer chains during the course of liquid droplet formation can slow down the fibrillation of HPMC. At lower hydroxypropyl content (i.e., for 65SH-4000), the liquid droplets are expected to be less hydrated than those at larger hydroxypropyl content, suppressing diffusion even further as reflected in the power B.

Paper Soft Matter

Conclusion

Thermoresponsive polymers continue to be critical to the expansion of our understanding of polymer physics as well as to the production of novel, smart materials.⁵⁹ Here, we have reported on the dynamics and mechanisms for the phase transition of cellulosic derivatives. We demonstrated that at elevated temperatures above the LCST, HPC phase separates into liquid droplets which can expel water and shrink in size when the molecular weight is sufficiently large. Due to the presence of hydroxypropyl groups, HPC droplets are flexible and can swell during cooling from high temperatures to the LCST, transitioning to a solvated state with no thermal hysteresis. Conversely, MC was shown to self-assemble into fibrils via a slow diffusive process. Unlike HPC droplets, a significant hysteresis exists in the phase transition of MC during heating and cooling. However, the presence of hydroxypropyl groups reduced the hysteresis between the phase transition during heating and cooling as shown for HPMC. We quantitatively showed that the reduction of hysteresis is due to an alteration in the fibrillation mechanism: instead of a diffusive growth rate in bulk, HPMC fibrils are formed through liquid droplets, resulting in limited fibrillation and shorter lengths compared to those for MC fibrils. These findings can be further used to design a new generation of thermoresponsive cellulosic gels.

Materials and methods

Materials preparation

Five grades of hydroxypropyl cellulose (HPC) were kindly provided by Nippon Soda Co. Ltd, Japan. Five grades of methyl cellulose (MC) and two grades of hydroxypropyl methylcellulose (HPMC) were kindly provided by Shin-Etsu Chemical Co. Ltd, Japan. These materials required no further purification as evidenced by small-angle neutron scattering and micro differential scanning calorimetry assessments.60 The properties of these naturally-derived polymers were provided by their manufacturers as listed in Table 1. The hydroxyproxy content in HPC and methoxy content in MC results in a degree of substitution of 2.3⁶¹ and 1.8,⁶² respectively. Aqueous solutions of these polymers were prepared at a desired concentration in the range of 0.001 wt% to 2.6 wt% by stirring the mixture for several hours followed by overnight storage in a fridge at 5 °C.

Dynamic light scattering (DLS)

Scattering intensity of polymer solutions, I(t), was measured by an Anton Paar Litesizer 500 with a laser light of wavelength 658 nm generated by a single-frequency laser diode at 40 mW. For macromolecules undergoing Brownian motion, we have fitted an exponential decay function, $1 + a \exp(-2\Gamma \tau)$, to the normalized autocorrelation function, $g_2(\tau) = \langle I(t)I(t+\tau)\rangle/\langle I(t)\rangle^2$, to compute the decay constant, Γ . ⁶⁵ Sweeping temperature on the given polymer solution from 30 $^{\circ}\text{C}$ to 80 $^{\circ}\text{C}$ and back to 26 $^{\circ}\text{C}$ at a constant rate of 0.2 $^{\circ}$ C min⁻¹, we computed Γ for every 2 $^{\circ}$ C interval. The geometrical shape of particle dictates the light scattering. For symmetric particles, e.g., HPC droplets, the scattered light from particles is also symmetric, whereas it is asymmetric for non-spherical particles such as MC fibrils. Fig. S3 in the ESI†, shows how scattered light from HPC droplets and MC fibrils depend on the angular position of detector with respect to the sample cell. While the detector for scattered light could be set at three different angles, 15°, 90°, and 175°, the side angle (i.e., 90°) has been used in all measurements unless stated otherwise. Therefore, the Stokes-Einstein model⁶⁵ has been used to determine the diameter of HPC droplets, but our computations for Γ are used to determine the characteristic length of MC fibrils, l, assuming that $l \sim 1/\Gamma$. Fig. S4 and S5 in the ESI†, show the correlation function and the computation of Γ from fitted exponential decay functions for selected cases. A dimensional factor is required to convert Γ to absolute values of fibril length. Instead, we obtained the characteristic length of fibrils in dimensionless forms of l/l_0 , l/l_{max} , or $(l - l_0)/l_{max}$, where l_0 and l_{max} are the characteristic length of fibrils at the LCST and hydrated state, respectively. To obtain the time series measurements, the polymer solution was heated up to the lower critical solution temperature (LCST) of given polymer at a constant rate of 0.2 °C min⁻¹, and then the scattering intensity was measured every 3 min for 10 h while maintaining temperature constant at the LCST. In all light scattering measurements, the light transmittance was also simultaneously measured.

Differential scanning calorimetry (DSC)

Calorimetric analysis of polymer solutions was carried out using a TA Instruments Discovery 2500 Differential Scanning Calorimeter equipped with an RCS90 cooler. To suppress water vaporization during heating, stainless steel high-volume pans equipped with an internal O-ring (TA part number 900825.902) were used, which can withstand an internal pressure of 4.1 MPa. Each pan was filled with 80-90 μL of aqueous solution containing 2 to 3 wt% polymer, after which the pan was hermetically sealed. The sample pan was loaded into the DSC along with a reference pan containing an equivalent volume of deionized water. This helped to stabilize the baseline heat flow signal. Heat flow to each sample was continuously measured as temperature was cycled from 10 $^{\circ}$ C to 90 $^{\circ}$ C and back to 20 $^{\circ}$ C at a rate of 1 °C min⁻¹. Multiple heating and cooling cycles were carried out for selected samples to check the reproducibility of the thermal events. Sample and reference pans were weighed before and after analysis to verify that no mass loss occurred during analysis. The DSC was calibrated with the appropriate pans and heating rate according to standard procedures using indium and sapphire standards. Control experiments were performed with deionized water to ensure that no thermal events were observed during heating and cooling at the relevant temperature range.

Atomic force microscopy (AFM)

AFM has been conducted to reveal the morphology of phaseseparated MC and HPC polymers. To prepare AFM samples, 0.001 wt% aqueous solutions of MC (SM-8000) and HPC

(HPC-H) (see Table 1) were heated up to 70 °C at a rate of 1 °C min⁻¹. Within a few minutes after reaching the desired temperature, approximately 50 µL of hot sample was pipetted onto a silicon wafer that was also heated to 70 $^{\circ}$ C. The substrate was held at 70 °C until the deposited drop evaporated completely, after which it was cooled to room temperature through natural convection prior scanning. AFM images were acquired by a Bruker Dimension ICON3 on a tapping mode with a force constant of 2 N m⁻¹ and a resonance frequency of 70 kHz. Gwyddion software was used to analyze and process the AFM images.

Abbreviations

AFM Atomic force microscopy DLS Dynamic light scattering DS Degree of substitution

DSC Differential scanning calorimetry

HPC Hydroxypropyl cellulose

Hydroxypropyl methylcellulose **HPMC** LCST Lower critical solution temperature

MC Methyl cellulose MW Molecular weight

Conflicts of interest

The authors declare no competing financial interest.

Acknowledgements

This work was supported by the Materials Research Science and Engineering Center Program by National Science Foundation through the Princeton Center for Complex Materials (PCCM) (DMR-2011750). N. B. acknowledges support of the PCCM postdoctoral fellowship.

References

- 1 E. Kontturi, P. Laaksonen, M. B. Linder, Nonappa, A. H. Gröschel, O. J. Rojas and O. Ikkala, Adv. Mater., 2018, 30, 1703779.
- 2 D. Zhao, Y. Zhu, W. Cheng, G. Xu, Q. Wang, S. Liu, J. Li, C. Chen, H. Yu and L. Hu, Matter, 2020, 2, 390-403.
- 3 A. A. Aldana, S. Houben, L. Moroni, M. B. Baker and L. M. Pitet, ACS Biomater. Sci. Eng., 2021, 7, 4077-4101.
- 4 X. Cui, J. J. L. Lee and W. N. Chen, Sci. Rep., 2019, 9, 18166.
- 5 T. Arfin, in Sustainable Nanocellulose and Nanohydrogels from Natural Sources, Micro and Nano Technologies, ed. F. Mohammad, H. A. Al-Lohedan and M. Jawaid, Elsevier, 2020, pp. 255-274.
- 6 Y.-J. Kim and Y. T. Matsunaga, J. Mater. Chem. B, 2017, 5, 4307-4321.
- 7 X. Yang, G. Liu, L. Peng, J. Guo, L. Tao, J. Yuan, C. Chang, Y. Wei and L. Zhang, Adv. Funct. Mater., 2017, 27, 1703174.

- 8 Y. Ding, Y. Yan, Q. Peng, B. Wang, Y. Xing, Z. Hua and Z. Wang, ACS Appl. Polym. Mater., 2020, 2, 3259-3266.
- 9 C. Nakamura, T. Yamamoto, K. Manabe, T. Nakamura, Y. Einaga and S. Shiratori, Ind. Eng. Chem. Res., 2019, 58, 6424-6428.
- 10 M. R. Yazdani, R. Ajdary, A. Kankkunen, O. J. Rojas and A. Seppälä, ACS Appl. Mater. Interfaces, 2021, 13, 6188-6200.
- 11 C. Brigham, in Chapter 3.22 Biopolymers: Biodegradable Alternatives to Traditional Plastics in Green Chemistry, ed. B. Török and T. Dransfield, Elsevier, 2018, pp. 753-770.
- 12 T. Kondo, A. Koschella, B. Heublein, D. Klemm and T. Heinze, Carbohydr. Res., 2008, 343, 2600-2604.
- 13 Y. Nishiyama, P. Langan and H. Chanzy, J. Am. Chem. Soc., 2002, 124, 9074-9082.
- 14 D. Klemm, B. Heublein, H.-P. Fink and A. Bohn, Angew. Chem., Int. Ed., 2005, 44, 3358-3393.
- 15 Y. Li, X. Liu, Y. Zhang, K. Jiang, J. Wang and S. Zhang, ACS Sustainable Chem. Eng., 2017, 5, 3417-3428.
- 16 B. Lindman, G. Karlström and L. Stigsson, J. Mol. Liq., 2010, **156**, 76-81.
- 17 X. Ju, M. Bowden, E. E. Brown and X. Zhang, Carbohydr. Polym., 2015, 123, 476-481.
- 18 T. G. Majewicz, P. E. Erazo-Majewicz and T. J. Podlas, Encyclopedia of Polymer Science and Technology, 2002.
- 19 C. G. Otoni, M. v Lorevice, M. R. de Moura and L. H. C. Mattoso, Carbohydr. Polym., 2018, 185, 105-111.
- 20 T. Funami, Y. Kataoka, M. Hiroe, I. Asai, R. Takahashi and K. Nishinari, Food Hydrocolloids, 2007, 21, 46-58.
- 21 W. Koch, Ind. Eng. Chem., 1937, 29, 687-690.
- 22 M. L. Coughlin, L. Liberman, S. P. Ertem, J. Edmund, F. S. Bates and T. P. Lodge, Prog. Polym. Sci., 2021, 112, 101324.
- 23 R. Bodvik, A. Dedinaite, L. Karlson, M. Bergström, P. Bäverbäck, J. S. Pedersen, K. Edwards, G. Karlsson, I. Varga and P. M. Claesson, Colloids Surf., A, 2010, 354, 162-171.
- 24 T. Chatterjee, A. I. Nakatani, R. Adden, M. Brackhagen, D. Redwine, H. Shen, Y. Li, T. Wilson and R. L. Sammler, Biomacromolecules, 2012, 13, 3355-3369.
- 25 L. Li, P. M. Thangamathesvaran, C. Y. Yue, K. C. Tam, X. Hu and Y. C. Lam, Langmuir, 2001, 17, 8062-8068.
- 26 T. Tang, V. Castelletto, P. Parras, I. W. Hamley, S. M. King, D. Roy, S. Perrier, R. Hoogenboom and U. S. Schubert, Macromol. Chem. Phys., 2006, 207, 1718-1726.
- 27 R. Pires-Oliveira, J. Tang, A. M. Percebom, C. L. Petzhold, K. C. Tam and W. Loh, Langmuir, 2020, 36, 15018-15029.
- 28 L. Mäkinen, D. Varadharajan, H. Tenhu and S. Hietala, Macromolecules, 2016, 49, 986-993.
- 29 K. Jain, R. Vedarajan, M. Watanabe, M. Ishikiriyama and N. Matsumi, Polym. Chem., 2015, 6, 6819-6825.
- 30 N. Zhang, S. Salzinger and B. Rieger, Macromolecules, 2012, **45**, 9751-9758.
- 31 E. G. Gharakhanian and T. J. Deming, J. Phys. Chem. B, 2016, 120, 6096-6101.
- 32 M. Glassner, K. Lava, V. R. de la Rosa and R. Hoogenboom, J. Polym. Sci., Part A: Polym. Chem., 2014, 52, 3118-3122.

- 33 N. Liu, C.-H. Ma, R.-W. Sun, J. Huang, C. Li and Z.-Q. Wu, Polym. Chem., 2017, 8, 2152-2163.
- 34 A. Ianiro, H. Wu, M. M. J. van Rijt, M. P. Vena, A. D. A. Keizer, A. C. C. Esteves, R. Tuinier, H. Friedrich, N. A. J. M. Sommerdijk and J. P. Patterson, Nat. Chem., 2019, 11, 320-328.
- 35 Y. Tezuka, K. Imai, M. Oshima and T. Chiba, Macromolecules, 1987, 20, 2413-2418.
- 36 T. Kyu and P. Mukherjee, Liq. Cryst., 1988, 3, 631-644.
- 37 S. Costanzo, R. Pasquino, R. Donato and N. Grizzuti, Polymer, 2017, 132, 157-163.
- 38 J. R. Lott, J. W. McAllister, M. Wasbrough, R. L. Sammler, F. S. Bates and T. P. Lodge, Macromolecules, 2013, 46, 9760-9771.
- 39 J. W. McAllister, P. W. Schmidt, K. D. Dorfman, T. P. Lodge and F. S. Bates, Macromolecules, 2015, 48, 7205-7215.
- 40 J. R. Lott, J. W. McAllister, S. A. Arvidson, F. S. Bates and T. P. Lodge, Biomacromolecules, 2013, 14, 2484-2488.
- 41 P. W. Schmidt, S. Morozova, S. P. Ertem, M. L. Coughlin, I. Davidovich, Y. Talmon, T. M. Reineke, F. S. Bates and T. P. Lodge, Macromolecules, 2020, 53, 398-405.
- 42 P. W. Schmidt, S. Morozova, P. M. Owens, R. Adden, Y. Li, F. S. Bates and T. P. Lodge, Macromolecules, 2018, 51, 7767-7775.
- 43 W. Huang, R. Ramesh, P. K. Jha and R. G. Larson, Macromolecules, 2016, 49, 1490-1503.
- 44 V. Sethuraman and K. D. Dorfman, Phys. Rev. Mater., 2019, 3, 55601.
- 45 V. V. Ginzburg, R. L. Sammler, W. Huang and R. G. Larson, J. Polym. Sci., Part B: Polym. Phys., 2016, 54, 1624-1636.
- 46 W. Huang, I. S. Dalal and R. G. Larson, J. Phys. Chem. B, 2014, 118, 13992-14008.
- 47 X. Li, F. S. Bates and K. D. Dorfman, Phys. Rev. Mater., 2017, 1, 25604.

- 48 T. P. Lodge, A. L. Maxwell, J. R. Lott, P. W. Schmidt, J. W. McAllister, S. Morozova, F. S. Bates, Y. Li and R. L. Sammler, Biomacromolecules, 2018, 19, 816-824.
- 49 J. P. A. Fairclough, H. Yu, O. Kelly, A. J. Ryan, R. L. Sammler and M. Radler, Langmuir, 2012, 28, 10551-10557.
- 50 S. Morozova, P. W. Schmidt, F. S. Bates and T. P. Lodge, Macromolecules, 2018, 51, 9413-9421.
- 51 V. Sethuraman and K. D. Dorfman, Phys. Rev. Mater., 2020, 4, 85601.
- 52 S. Morozova, Polym. Int., 2020, 69, 125-130.
- 53 M. Martin-Pastor and E. Stoyanov, J. Polym. Sci., 2020, 58, 1632-1641.
- 54 M. Dušková-Smrčková and K. Dušek, ACS Macro Lett., 2019, 8, 272-278.
- 55 L. Li, Macromolecules, 2002, 35, 5990-5998.
- 56 F. Garcia Quiroz, N. K. Li, S. Roberts, P. Weber, M. Dzuricky, I. Weitzhandler, Y. G. Yingling and A. Chilkoti, Sci. Adv., 2019, 5, eaax5177.
- 57 M. Mosharraf and C. Nyström, Int. J. Pharm., 1995, 122, 35-47.
- 58 B. A. Miller-Chou and J. L. Koenig, Prog. Polym. Sci., 2003, 28, 1223-1270.
- 59 J. Zhao, V. E. Lee, R. Liu and R. D. Priestley, Annu. Rev. Chem. Biomol. Eng., 2019, 10, 361-382.
- 60 L. Li, Macromolecules, 2002, 35, 5990-5998.
- 61 K. Kimura, T. Shigemura, M. Kubo and Y. Maru, Die Makromolekulare Chemie, 1985, 186, 61-70.
- 62 K. Arai, Y. Horikawa, T. Shikata and H. Iwase, RSC Adv., 2020, 10, 19059-19066.
- 63 T. Kato, T. Tokuya and A. Takahashi, Kobunshi Ronbunshu, 1982, 39, 293-298.
- 64 H. Andersson, H. Häbel, A. Olsson, S. Sandhagen, C. von Corswant, J. Hjärtstam, M. Persson, M. Stading and A. Larsson, Int. J. Pharm., 2016, 511, 223-235.
- 65 J. Stetefeld, S. A. McKenna and T. R. Patel, Biophys. Rev., 2016, 8, 409-427.